



HAL
open science

Towards manufactured lattice structures: a comparison between layout and topology optimization

Enrico Stragiotti, François-Xavier Irisarri, Cédric Julien, Joseph Morlier

► To cite this version:

Enrico Stragiotti, François-Xavier Irisarri, Cédric Julien, Joseph Morlier. Towards manufactured lattice structures: a comparison between layout and topology optimization. AeroBest 2021 International Conference on Multidisciplinary Design Optimization of Aerospace Systems. Book of proceedings, ECCOMAS, Jul 2021, Lisbon, Portugal. pp.229-244. hal-03384893

HAL Id: hal-03384893

<https://hal.science/hal-03384893>

Submitted on 19 Oct 2021

HAL is a multi-disciplinary open access archive for the deposit and dissemination of scientific research documents, whether they are published or not. The documents may come from teaching and research institutions in France or abroad, or from public or private research centers.

L'archive ouverte pluridisciplinaire **HAL**, est destinée au dépôt et à la diffusion de documents scientifiques de niveau recherche, publiés ou non, émanant des établissements d'enseignement et de recherche français ou étrangers, des laboratoires publics ou privés.

TOWARDS MANUFACTURED LATTICE STRUCTURES: A COMPARISON BETWEEN LAYOUT AND TOPOLOGY OPTIMIZATION

Enrico Stragiotti¹, François-Xavier Irisarri¹, Cédric Julien¹ and Joseph Morlier²

1: ONERA - The French Aerospace Lab
DMAS - Département matériaux et structures
92320 Châtillon, France
{enrico.stragiotti, francois-xavier.irisarri, cedric.julien}@onera.fr

2: ICA - Institut Clément Ader
ISAE - SUPAERO
31400 Toulouse, France
joseph.morlier@isae-supero.fr

Abstract. *The repetitive nature of cellular lattice structures brings various interesting features among which fast assembly and repair time, reduced tooling, and manufacturing costs are major advantages. Additionally, as the mechanical performances of the structure are heavily influenced by the topology and materials of the cell, the designers can optimize the cell to tailor the structure for various scenarios. In this paper, we discuss and compare two relevant structural optimization methods for lattice structures: topology optimization and layout optimization. In the first part of the article, we presented an innovative cellular topology optimization formulation that minimizes the structural mass taking into account the internal stresses. The cellular implementation is based on the full-scale method called variable linking. In the second part, a qualitative comparison of topology and layout optimization is carried out, analysing the strength and the weakness of the two methods when applied to a lattice structure context.*

Keywords: Lattice Structures, Topology Optimization, Layout Optimization, Stress-Constrained Optimization, Structural Optimization

1 INTRODUCTION

The reduction of weight and the minimization of environmental cost are some of the major subjects on which every aerospace company is focusing at this moment. One of the fields that could significantly contribute to achieving this goal is structural optimization. The efficient use of the material in complex components helps to achieve enhanced mechanical performances, failure-safe behaviour, and minimum weight. The general aim of our study is to develop an optimization methodology for cellular lattice structures. The repetitive nature of such structures brings various interesting features among which fast assembly and repair time, reduced tooling, and manufacturing costs are major advantages. Additionally, as the mechanical performances of the structure are heavily influenced by the topology and materials of the cell, the designers can optimize the cell to tailor the structure for various scenarios. For instance, cellular lattice structures have been shown to be interesting candidates for innovative wing structures [1–3].

In this paper, we discuss and compare two relevant structural optimization methods for lattice structures: topology optimization [4, 5] and layout optimization [6, 7]. Topology optimization considers the design domain as a continuum, in which each location may or may not have a material assigned to it, while layout optimization is applied to a ground structure, a discrete environment. The latter is an algorithm that identifies the optimal section sizes and connectivity of the members of a truss. To benchmark the two algorithms, a stress-constrained multi-scale optimization is set up, in which the objective is to minimize the volume of the structure. The performances, shape, and manufacturability of the optimized results are compared.

The literature of cellular structure optimization is mainly divided into full-scale and multi-scale approaches [8]. This paper focuses on cellular structures for which there is no clear scale separation between the repeating pattern and the full structure. Thus, we are from now on only considering full-scale approaches. Compared to multi-scale approaches, full-scale approaches are less covered in the literature.

While full-scale approaches have been already applied to compliance minimization [8] and mechanism design [9] problems, there are, to the authors' knowledge, no published studies on stress-constrained volume minimization full-scale optimization.

This paper is structured in the following way: in Section 2 we present the stress-based volume minimization topology optimization problem [10] and its extension to cellular structures using the variable linking method [9, 11]. Cellular and non-cellular approaches are compared. In Section 3, layout optimization is compared in a qualitative way to topology optimization in the full-scale optimization framework. Concluding remarks are given in Section 4.

2 STRESS-BASED CELLULAR TOPOLOGY OPTIMIZATION

2.1 Stress-based Topology Optimization

Let Ω be a rectangular domain of dimensions X and Y , containing respectively N_x and N_y linear 4-nodes elements. Following the classic topology optimization theory, a density variable ρ is linked to every element of the structure. The density variable can span between zero and one and represents void or full material, respectively. The classic objective function for a topology optimization problem is the minimization of the compliance [5]. Instead of finding the stiffest structure with a fixed volume fraction, we decided in

this paper to reformulate the compliance minimization problem and search for the lowest volume structure with a local strength constraint.

Three main difficulties may arise in solving this problem:

1. The stress constraints are defined only for the elements where $\rho_i > 0$, thus the set of constraints changes during the optimization. This class of problems are called mathematical programs with vanishing constraints (MPVCs) [12] and are known for being difficult to solve.
2. Is it known in the literature [13, 14] that MPVCs often suffer from *singular minima*: firstly observed on truss structure optimization [15], they are inaccessible to standard gradient-based optimizer, and they represent the *minima* of the optimization. This problem is often solved using a technique called *relaxation*.
3. The stress is a local measure, and thus a large set of constraints is generated when a reasonably fine mesh is used (one element, one constraint). This problem is often solved using a technique called *aggregation*.

The implementation of this paper is based on the use of a lower bound Kreisselmeier-Steinhauser (KS) function [16] to apply relaxation and aggregation at the same time [10]. One could formulate the normalized local stress constraint as:

$$g_j = \frac{\sigma_{VM,j}}{\sigma_l} - 1 \leq 0, \quad \forall j \in \Omega_{mat}(\boldsymbol{\rho}), \quad (1)$$

where $\Omega_{mat}(\boldsymbol{\rho})$ represents the design-dependent set of elements with a non-zero density, $\sigma_{VM,i}$ represents the equivalent von Mises stress for the element i , and σ_l is the maximum allowable equivalent von Mises stress. In this formulation all the stresses are evaluated using the microscopic stress formulation and assuming that there is no direct correlation between stress and density [17]. Indeed, the use of the macroscopic stress in volume minimization optimization problems creates all-void design [18]. The original set of constraints is reformulated into an equivalent design-independent set of constraints [19]:

$$\bar{g}_i = \tilde{\rho}_i g_i = \tilde{\rho}_i \left(\frac{\sigma_{VM,i}}{\sigma_l} - 1 \right) \leq 0, \quad \forall i \in \Omega. \quad (2)$$

Following the work developed by Verbart [10], the lower bound Kreisselmeier-Steinhauser function is used to approximate the local relaxed stress constraint maximum:

$$G_{KS}^l = \frac{1}{P} \ln \left(\frac{1}{N_e} \sum e^{P\bar{g}_i} \right) \quad \text{with } N_e = \text{number of elements } e \in \Omega. \quad (3)$$

Its main advantage over other different formulations is that it uses a single hyperparameter P to control the aggregation and the relaxation of the constraints.

The optimization problem is then written as:

$$\begin{aligned}
 (\mathbb{P}_1) : \quad \min_{\boldsymbol{\rho}} \quad & V = \frac{1}{V_0} \sum_{i \in \Omega} \tilde{\rho}_i v_i \\
 \text{s.t.} \quad & G_{KS}^l = \frac{1}{P} \ln \left(\frac{1}{N_e} \sum_{i \in \Omega} e^{P\bar{g}_i} \right) \leq 0 \\
 & \mathbf{KU} = \mathbf{F} \\
 & 0 \leq \rho_i \leq 1,
 \end{aligned} \quad (4)$$

where v_i represents the volume of the i -th element and the objective function V is the volume fraction occupied in the volume $V_0 = \sum v_i$. $\boldsymbol{\rho} = [\rho_1, \rho_2, \dots, \rho_{Ne}]^T$ represents the design variable of the optimization, while $\tilde{\boldsymbol{\rho}} = [\tilde{\rho}_1, \tilde{\rho}_2, \dots, \tilde{\rho}_{Ne}]^T$ represents the physical density, obtained after filtering and projection of $\boldsymbol{\rho}$. $\mathbf{KU} = \mathbf{F}$ is the state equation of the problem and define the elastic response of the structure to an external load $\mathbf{F} = [f_1, f_2, \dots, f_{Ne}]^T$. The global stiffness matrix \mathbf{K} is assembled from the element stiffness matrix $\mathbf{K} = \sum_{i \in \Omega} \mathbf{K}_{e,i}$ and $\mathbf{K}_{e,i} = E_i \mathbf{K}_{e,0}$ where $\mathbf{K}_{e,0}$ represents the stiffness matrix relative to the chosen type of element and $E_i(\tilde{\rho}_i)$ the Young's modulus of the element. In this paper, we use the Solid Isotropic Material Interpolation with Penalization (SIMP) [20] approach to calculate $E_i(\tilde{\rho}_i)$. It is governed by the equation:

$$E_i = E_{\min} + \tilde{\rho}_i^p (E_0 - E_{\min}), \quad (5)$$

where the parameter p penalizes the intermediate densities and pushes the result to a black and white result. E_0 is the young's modulus of the full material and E_{\min} is a small value that avoid the global stiffness matrix \mathbf{K} from being singular when $\tilde{\rho}_i = 0$. In this paper we set $E_0 = 1$, $E_{\min} = 10^{-9}$ and $p = 3$.

To solve the problems linked to the mesh discretization, such as the mesh dependence or the checkerboard problem, a standard linear spatial filter based on the 2D convolution operator [21] is used. The weight function $w(d)$ is defined as:

$$w(d_j) = R - d_j, \quad j \in \mathbb{N}_{i,R}, \quad (6)$$

where $\mathbb{N}_{i,R}$ represent the set of elements lying within a circle of radius R centred on the i -th element. d_j is the distance of the j -th element to the centre of the filter. The filtered values of the design variable calculated as:

$$\tilde{\rho}_i = \frac{\sum_{j \in \mathbb{N}_{i,R}} w(d_j) v_j \rho_j}{\sum_{j \in \mathbb{N}_{i,R}} w(d_j) v_j}. \quad (7)$$

The derivative of the filtered densities $\tilde{\boldsymbol{\rho}}$ with respect to the design variables $\boldsymbol{\rho}$ is:

$$\frac{\partial \tilde{\rho}_i}{\partial \rho_j} = \frac{w(d_j) v_j}{\sum_{j \in \mathbb{N}_{i,R}} w(d_j) v_j}. \quad (8)$$

As the filtering phase usually produces a large quantity of grey element, a smooth projection technique based on the \tanh function is implemented [22]:

$$\tilde{\rho}_j = \frac{\tanh(\beta\eta) + \tanh(\beta(\tilde{\rho}_j - \eta))}{\tanh(\beta\eta) + \tanh(\beta(1 - \eta))}, \quad (9)$$

where β is a parameter that define the slope of this approximation function and η is the threshold value. It is important to note that this type of projection is not volume conservative for all values of η . In order to stay conservative we decided to have a volume-increasing filter, and a value of $\eta = 0.4$ is chosen in this work [23]. The sensitivity of the physical densities $\tilde{\boldsymbol{\rho}}$ with respect to the filtered $\tilde{\boldsymbol{\rho}}$ can be written as:

$$\frac{\partial \tilde{\rho}_j}{\partial \tilde{\rho}_j} = \beta \frac{1 - \tanh^2(\beta(\tilde{\rho}_j - \eta))}{\tanh(\beta\eta) + \tanh(\beta(1 - \eta))}. \quad (10)$$

Using the chain rule is possible to write:

$$\frac{\partial f}{\partial \rho_i} = \sum_{j \in \mathbb{N}_{i,R}} \frac{\partial f}{\partial \tilde{\rho}_j} \frac{\partial \tilde{\rho}_j}{\partial \rho_i}, \quad (11)$$

where f represent a generic function.

Using the adjoint method the sensitivity analysis of \mathbb{P}_1 with respect to the physical densities $\tilde{\rho}$ become:

$$\frac{\partial V}{\partial \tilde{\rho}_i} = \frac{v_i}{V_0}, \quad (12)$$

$$G_{KS}^l = g(\tilde{\rho}, \mathbf{U}(\tilde{\rho})) \iff \frac{dg}{d\tilde{\rho}_i} = \frac{\partial g}{\partial \tilde{\rho}_i} + \frac{\partial g}{\partial \mathbf{U}}^T \frac{d\mathbf{U}}{d\tilde{\rho}_i} \quad (13)$$

$$\frac{\partial g}{\partial \mathbf{U}} = \frac{\rho_i}{\sigma_l \sigma_i} e^{P\tilde{g}_i} |\mathbf{S}_i|_g \mathbf{U} \quad (14)$$

$$\frac{dg}{d\tilde{\rho}_i} = \left(\frac{\sigma_{VM,j}}{\sigma_l} - 1 \right) \frac{e^{P\tilde{g}_j}}{\sum_k e^{P\tilde{g}_k}} - \boldsymbol{\lambda} \left(-P\tilde{\rho}_i^{P-1} \mathbf{K}_{e,i} \right) \mathbf{U}, \quad (15)$$

where $\boldsymbol{\lambda}$ is the adjoint vector that solves the adjoint system $\mathbf{K}\boldsymbol{\lambda} = \partial g / \partial \mathbf{U}$ and $|\mathbf{S}_i|_g$ represents the matrix that links local to global coordinates (in the same way we linked $\mathbf{K}_{e,i}$ to \mathbf{K}).

2.2 Cellular approach — Variable linking scheme

The cellular approach is implemented using a variable linking scheme on a structured grid [11]. The design variables $\boldsymbol{\kappa} = [\kappa_1, \kappa_2, \dots, \kappa_{n_e}]^T$ where $n_e = n_x \times n_y$ is the number of elements are defined in a design cell Ω_c . $\boldsymbol{\kappa}$ is defined on every finite element of Ω_c and linked to the density ρ over the entire structure Ω (see Figure 1). Following the nomenclature of Wu [8], this method can be described as a full-scale approach with repeated pattern.

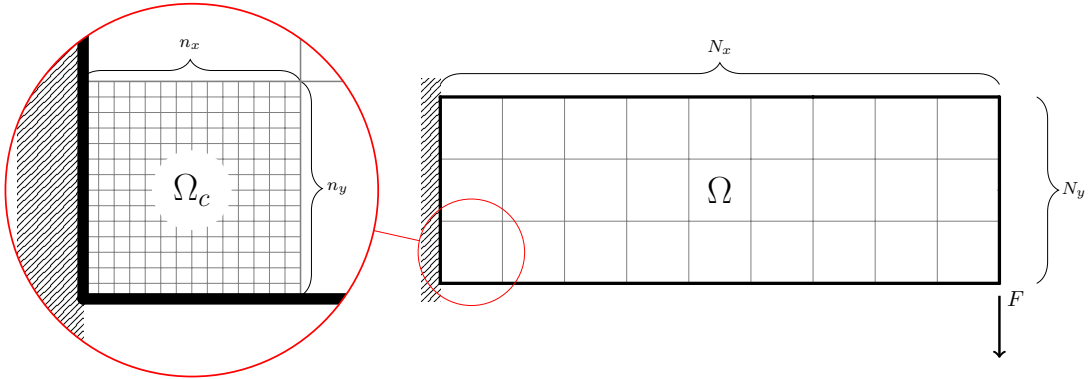


Figure 1: Design domain and boundary condition for a cantilever beam using a variable linking scheme. The design variables $\boldsymbol{\kappa}$ inside the domain Ω_c are linked to the structure Ω to evaluate the state equation.

A common way to implement this approach is by defining a mapping matrix \mathbf{G} [9] and retrieving the optimization densities by using the following relation $\boldsymbol{\rho} = \mathbf{G}\boldsymbol{\kappa}$. \mathbf{G} is a sparse $N_e \times n_e$ matrix where, if the design variable κ_j is linked to the optimization variable ρ_i , then $\mathbf{G}(i, j) = 1$. Problem \mathbb{P}_1 is then reformulated as follows:

$$\begin{aligned}
(\mathbb{P}_1^*) : \quad & \min_{\boldsymbol{\kappa}} \quad V = \frac{1}{V_0} \sum_{k \in \Omega_c} \kappa_k v_k \\
\text{s.t.} \quad & G_{KS}^l = \frac{1}{P} \ln \left(\frac{1}{N} \sum_{i \in \Omega} e^{P \bar{g}_i} \right) \leq 0 \\
& \mathbf{K}\mathbf{U} = \mathbf{F} \\
& 0 \leq \kappa_k \leq 1 \\
& \boldsymbol{\rho} = \mathbf{G}\boldsymbol{\kappa}.
\end{aligned} \tag{16}$$

where Ω_c represents the design cell (see Figure 1).

The sensitivity of the objective function and the constraints with respect to the design variables are calculated as [9]:

$$\frac{\partial f}{\partial \kappa_k} = \mathbf{G}^T \frac{\partial f}{\partial \bar{\rho}_i}. \tag{17}$$

The full sensitivities can then be calculated combining Equation 11, 12, 15 and 17. Derivatives are smooth and then suitable for gradient descent optimization algorithms.

2.3 Numerical results and discussion

The cantilever beam, together with the L-shape domain, represents one of the standard load cases used to assess the performance of a stress-constrained topology optimization [10]. The mesh used to discretize the full structure is made up by 400×200 linear 4-nodes

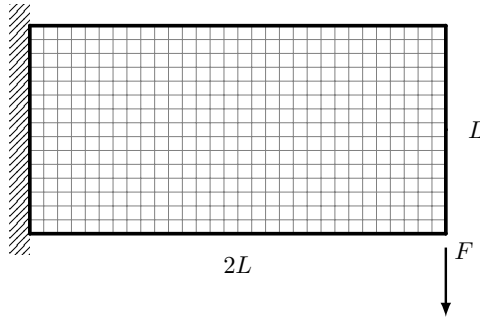


Figure 2: Cantilever beam load case. The domain is discretized into 400×200 linear quadratic elements.

elements (see Figure 2). The punctual load is distributed over 10 elements to avoid stress concentrations.

Problem 16 is solved for four different numbers of design cells (1×1 , 2×1 , 4×2 , and 8×4 cells). It is important to note that the full structure mesh is the same for all the cases, while the design space Ω_c shrinks down as more and more cells are added.

The optimizing algorithm chosen is the Method of Moving Asymptotes (MMA) [24]. The parameter called *movelimit* is set to 0.1. The other algorithm's parameters are set to their default value. More information on the implementation of the *movelimit*

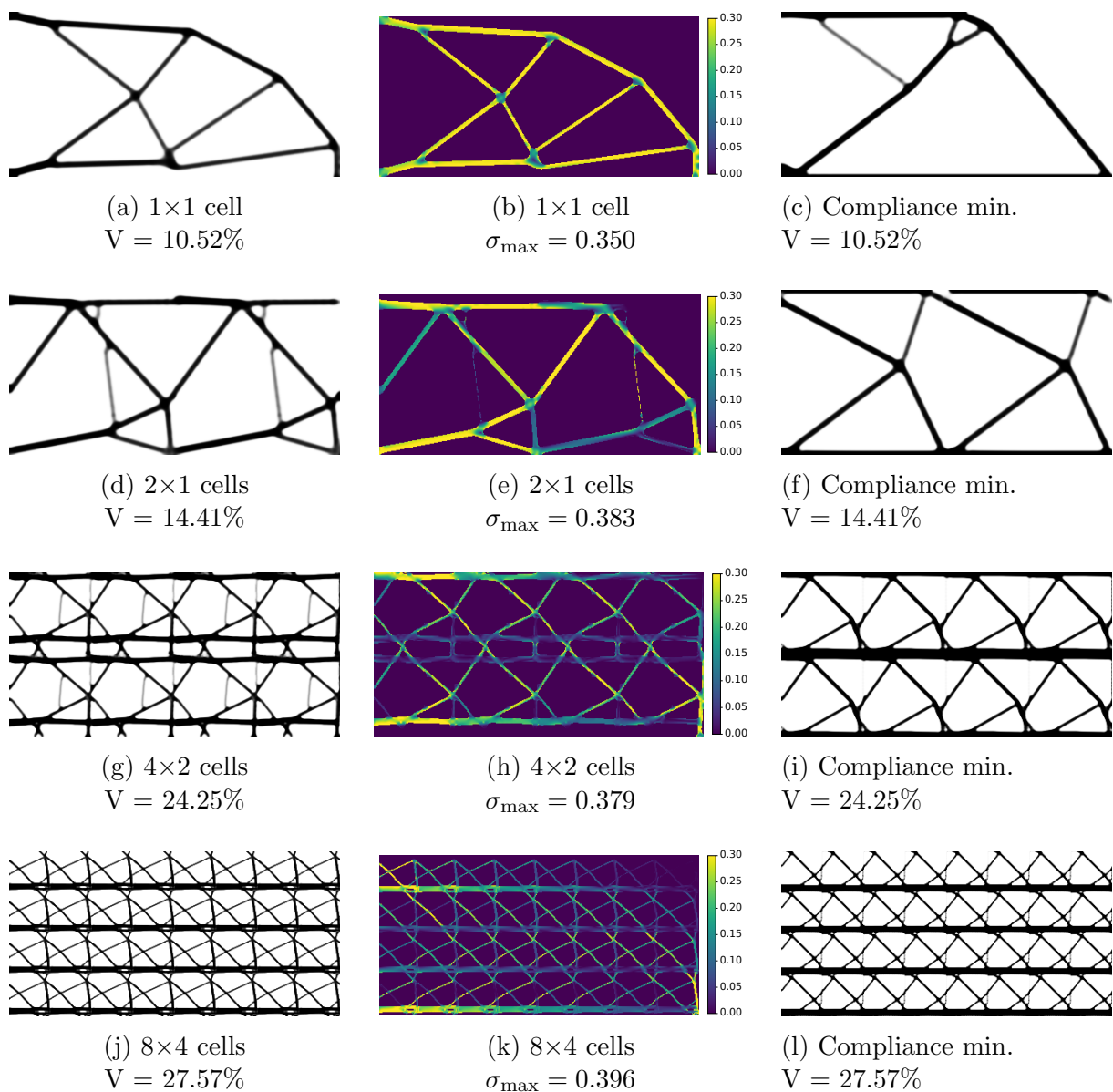


Figure 3: Topology optimization results. The first column presents the volume minimization density results. The central subfigures present the equivalent von Mises stress of the four load cases for the elements with a physical density $\tilde{\rho} > 0.5$. The last column presents the density of the results of the compliance minimization. The volume used as a constraint is the same found by the volume minimization.

parameter can be found on the original paper by Verbart [10]. A continuation scheme for the aggressiveness of the projection parameter β is set to increase by one every 200 iterations, the number of max iteration is set to 3000, the stopping criteria is calculated as $\|r_k\|_2/\sqrt{N_e}$ on the physical densities $\tilde{\rho}$ [23], and it is set to 10^{-4} . The aggregation parameter P is set to 32.

The isotropic material used for the optimization has been modelled with $E = 1$, $\nu = 0.3$ and the maximum allowable stress is set to $\sigma_L = 0.3$.

To evaluate the quality of the solutions, we evaluate the Measure of Non-Discreteness [25], where results near-zero mean a completely black and white design.

$$M_{nd} = \frac{\sum_e 4\tilde{\rho}_e(1 - \tilde{\rho}_e)}{n} \times 100\%. \quad (18)$$

Our optimization take into account only the linear behaviour of the structure.

Mesh size	Cells	Design Space	Volume	Max stress	M_{nd}
400x200	1x1	400x200	10.52%	0.350	4.45%
	2x1	200x200	14.41%	0.383	5.56%
	4x2	100x100	24.25%	0.379	10.22%
	8x4	50x50	27.57%	0.396	10.24%

Table 1: Numeric results of the variable linking approach applied to a topology optimization problem with stress constraints for increasing number of cells.

Looking at Table 1 and at Figure 3, we can summarize the results as:

- A first important remark is that the constraint function G_{KS}^l is always lower than the actual \bar{g} . As a consequence, the maximal von Mises stress is always greater than the actual allowable of 0.3. This is a known problem of this formulation [10].
- The optimized volume fraction increases with the number of cells, for a fixed maximal allowable stress (see Figure 4a). As the structure is divided into additional cells, the design space shrinks, constraining *de facto* our problem even more. This is a known drawback of cellular structures [8, 9].
- Classic volume minimization with stress constraints formulations tends to create full-stressed structures (see Figures 3a and b). When the linking variable approach is used, cells become less stressed, with the presence of elements that do not participate in the structural integrity of the cantilever. However, cellular structures are naturally more robust as they show structural redundancies and multiples stress paths. This opens up to the design of damage-tolerant structures [9].
- It is interesting to note that if the cells are stacked all one over the others, and we calculate the maximum stresses, one would find a full-stressed cell (see Figure 4b).

To assess the advantages of the volume minimization formulation, we compare the obtained results with those of compliance minimization. The compliance problem is formulated to accept a maximum volume fraction constraint, and we set that to the very same value found by the volume minimization. By doing so, it is possible to compare

maximum stresses and the compliance of the two linked formulations. Stress and compliance columns of Table 2 show the differences between the volume and the compliance minimization formulations. Figure 4a presents the general trend of the two different optimizations.

		Volume minimization		Compliance minimization	
Volume	Cells	Compliance	Max stress	Compliance	Max stress
10.52%	1x1	430.23 (1.19)	0.350 (1.0)	361.57 (1.0)	0.769 (2.19)
14.41%	2x1	412.52 (1.28)	0.383 (1.0)	320.89 (1.0)	0.783 (2.04)
24.25%	4x2	376.18 (1.34)	0.379 (1.0)	280.57 (1.0)	0.601 (1.58)
27.57%	8x4	369.50 (1.18)	0.396 (1.0)	312.52 (1.0)	1.470 (3.71)

Table 2: Comparison of the results obtained with the volume and the compliance minimization formulations. In the parenthesis, the results are normalized with respect to the maximum stress of the volume formulation and the compliance of the compliance formulation for a fixed volume fraction.

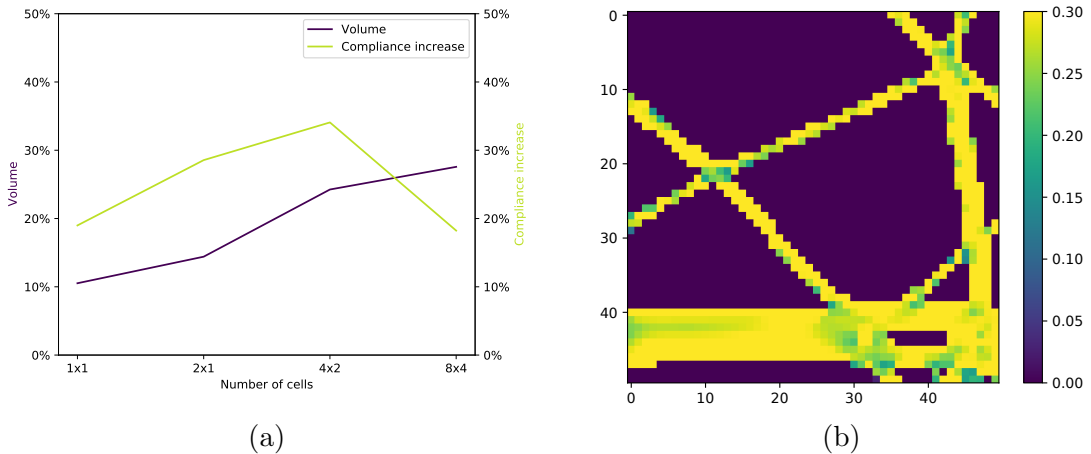


Figure 4: Figure 4a shows the trends of the optimization for the volume minimization formulation. The objective function is increasing with the number of cells. Figure 4b shows the 50×50 full-stressed cell, obtained superposing the maximum stress of all the cells inside Ω .

3 COMPARISON BETWEEN TOPOLOGY AND LAYOUT OPTIMIZATION

3.1 Cellular Layout Optimization

Layout optimization is a structural optimization algorithm that finds a near-optimal truss structure with respect to a given load case. Instead of working with a continuous domain as topology optimization does, layout optimization optimizes the sections and the connectivity of the members of a discrete ground structure [6]. The ground structure is defined as the full set of members that connect a grid of M points. For each member, we define a section a and a length l . As all the joints in the ground structure are treated as pin-joints, all the straight members face only tension or compression load.

Compared to the SIMP-based topology optimization described in Section 2, layout optimization seems appealing for the following reasons:

1. Looking at the pioneering works of Cramer [2] on ultralight structures as an example, we observe that the volume fraction of the cells is very low. The Ultem 100 and 200, the materials used by the authors to manufacture the cells, have a density of 1.42 g cm^{-3} . As the density of the cell structure is $5.566 \cdot 10^{-3} \text{ g cm}^{-3}$, we find a volume fraction of about 0.438%. It is known that such a low volume fraction on a regular, or even adaptive [26], mesh increases exponentially the number of elements required to correctly discretize the members in a topology optimization framework.
2. Even if the freedom of the design space offered by the continuum meshes used by topology optimization is higher, it is known that at these volume fractions and, especially if buckling constraints and manufacturing consideration are taken into account, the optimal topology is a truss structure [27]. Thus, for manufacturing easiness, one would prefer to directly work on a discrete ground structure. In addition to that, truss structures design naturally relies on constraints on maximum allowable stress, buckling, and maximum slenderness, which are all known for being difficult to implement on topology optimization.
3. Topology optimization needs massive computational resources to operate on large scale optimization [28], while layout optimization has been proven to work efficiently and fast for large aerospace applications [3].

The layout optimization problem is formulated as:

$$\begin{aligned}
 (\mathbb{P}_2) : \quad & \min_{\mathbf{a}} \quad V = \mathbf{l}^T \mathbf{a} \\
 & \text{s.t.} \quad \mathbf{B}\mathbf{q} = \mathbf{f} \\
 & \quad \quad -\sigma^- \mathbf{a} \leq \mathbf{q} \leq \sigma^+ \mathbf{a} \\
 & \quad \quad \mathbf{a} \geq 0,
 \end{aligned} \tag{19}$$

where V represent the structural volume evaluated as the product of the member lengths $\mathbf{l} = [l_1, l_2, \dots, l_N]^T$ and the design variables of the problem, the member sections $\mathbf{a} = [a_1, a_2, \dots, a_N]^T$. \mathbf{B} is a $2M \times N$ matrix containing the direction cosines of j -th member with respect to the i -th degree of freedom to calculate the nodal force equilibrium. M is the number of nodes and $N = M(M - 1)/2$ the number of members of a fully connected ground structure. $\mathbf{q} = [q_1, q_2, \dots, q_N]^T$ is a vector containing the internal member forces caused by the external load $\mathbf{f} = [f_1, f_2, \dots, f_M]^T$. σ^- and σ^+ are the compressive and tensile maximum allowable stress of the material, respectively. The resolution of Problem 19 produces complex structures made up of a multitude of small members that tends to the shapes of Michell structures [7, 29]. While it is known that these structures are nearly optimal, one would want to limit the complexity of the structure. Substituting \mathbf{l} with $\tilde{\mathbf{l}} = [l_1 + s, l_2 + s, \dots, l_N + s]^T$, one would penalize the appearance of small members [30]. $\tilde{\mathbf{l}}$ is called augmented member length and s is the joint cost. This approach mimics the mesh-independency regularization filter of topology optimization [5].

As formulated, Problem 19 represents a linear programming (LP) problem that can be efficiently solved by modern algorithms. In this work, we used the python library CVXPY [31].

The cellular approach of layout optimization is formulated following the same steps used for the topology optimization. The only implementation difference is that one should note that two contiguous cells share multiples members. So we added to the formulation an equality constraint between the upper and lower, and the right and left members of the cells (see Figure 5a). The problem is still linear after that reformulation.

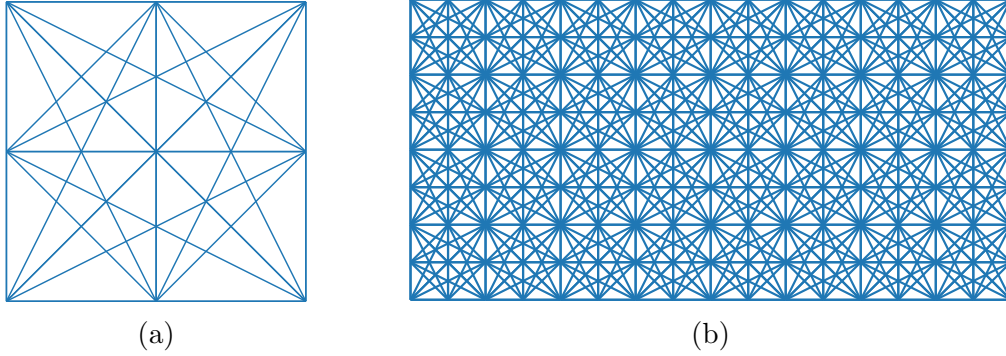
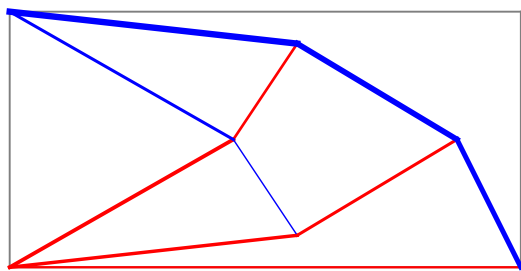


Figure 5: Figure 5a shows a 3-nodes cell of a ground structure made by the set of the 36 members that connect the nine points. Figure 5b present the 17×9 nodes ground structure made by 8×4 linked 3×3 cells.

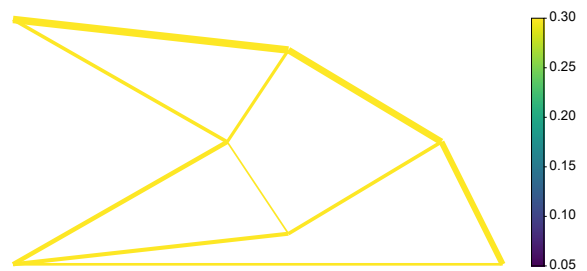
3.2 Numerical results and topology optimization comparison

The python implementation of Problem 19 is based on the 98-lines code provided by He [32]. The code has been extended by the authors to perform variable linking. The cantilever beam load case is used once again to assess the performance of the optimization algorithm. The analysis is performed on a fixed ground structure made up by 17×9 points, with a total of 11628 candidate members for the 1×1 case, 6444 for the 2×1 case, 2300 for the 4×2 case, and 996 for the 8×4 case (see Figure 5a and 5b). The maximum allowable stress is set to $\sigma_L = 0.3$ for tension and compression. The results of the optimization are presented in Figure 6. We can summarize them as:

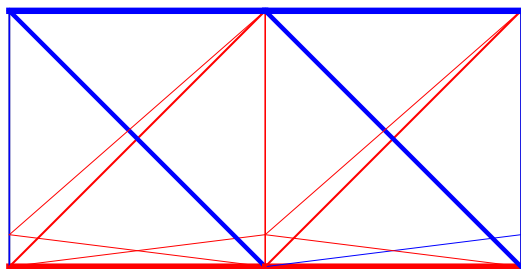
- Layout optimization presents the same trends of topology optimization concerning mechanical properties with respect to the number of cells. This is due to the restriction of the design space of the optimizer with the increase in the number of cells. It's interesting to note that changing the number of cells and thus the connectivity of the initial ground structure, not only the number of design variable, but the total number of members decrease as well.
- We find once again a full-stress design for the non-cellular case (see Figure 6b). The same considerations made for the full-stressed cell found in topology optimization hold for layout optimization as well.
- A direct comparison of the two formulations is non-trivial. In its most simple and diffused formulation, the mechanics of the material used for layout optimization follows the plastic design formulation. This means that the strain in the elastic region is considered negligible, and constant stress σ_y is therefore assumed for all non-zero strains. It is known that in stress-based topology optimization modifying Young's modulus E influences the solution found. Layout optimization and the



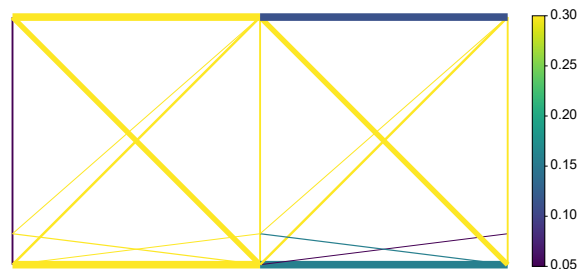
(a) 1×1 cell
 $V = 12446.12$



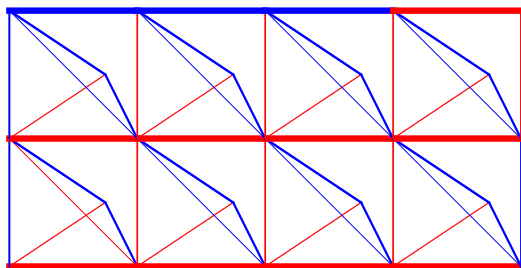
(b) 1×1 cell.



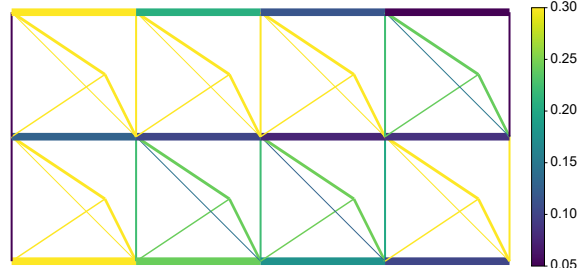
(c) 2×1 cells
 $V = 18598.48$



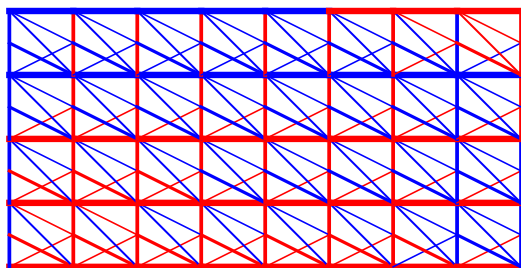
(d) 2×1 cells.



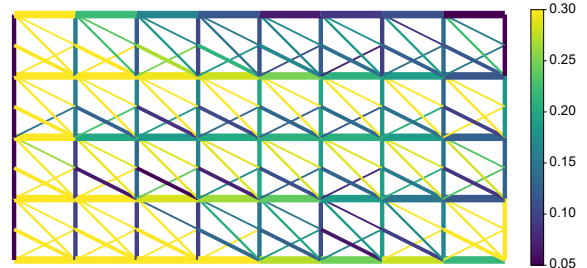
(e) 4×2 cells
 $V = 27916.67$



(f) 4×2 cells.



(g) 8×4 cells
 $V = 38259.26$



(h) 8×4 cells.

Figure 6: Layout optimization results. The colour of the member represents the load state, with red used for compression and blue for tension. The optimal section of the members is proportional to the thickness of the segments.

plastic material formulation, instead, aren't influenced by this parameter at all. It is thus difficult to compare the two formulations from a quantitative point of view.

- The topology of the optimal lattice structure could be constrained by the initial ground structure if the latter is too coarse.
- Compared to topology optimization, the computational time of layout optimization for a comparable number of design variables is between three and four orders of magnitude inferior. The lack of FEA and the simpler problem formulation reduce the iteration cost and the iteration number.

4 CONCLUDING REMARKS

In the first part of the article, we presented an innovative cellular topology optimization formulation that minimizes the structural mass of a 2D structure taking into account the internal stresses. The cellular implementation is based on the full-scale method called *variable linking*. The optimized structures are easier to manufacture and assemble and naturally damage tolerant, at the cost of a higher structural volume and compliance. In the second part, a qualitative comparison of topology and layout optimization applied to a cellular structure is carried out, analysing the strength and the weakness of the two methods.

The results obtained by the two methods exhibit the same general trends. The calculation cost of layout optimization is significantly lower than for topology optimization. Nonetheless, the plastic formulation in the layout optimization problem does not account for the material stiffness. With pin-jointed trusses and no material elastic behaviour, the obtained result is questionable from a mechanical point of view.

To do a proper quantitative comparison there is the need to add the material elastic behaviour to the layout optimization. A promising way to do that is to add what is known in the literature as a stress-strain compatibility [3]. Formulated in that way, the problem becomes non-linear, but the resulting structures will have a more meaningful mechanical behaviour.

REFERENCES

- [1] B. Jenett, S. Calisch, D. Cellucci, N. Cramer, N. Gershenfeld, S. Swei, and K. C. Cheung. Digital Morphing Wing: Active Wing Shaping Concept Using Composite Lattice-Based Cellular Structures. *Soft Robotics*, 4(1):33–48, Mar. 2017. doi:10.1089/soro.2016.0032.
- [2] N. B. Cramer, D. W. Cellucci, O. B. Formoso, C. E. Gregg, B. E. Jenett, J. H. Kim, M. Lendraitis, S. S. Swei, G. T. Trinh, K. V. Trinh, and K. C. Cheung. Elastic shape morphing of ultralight structures by programmable assembly. *Smart Materials and Structures*, 28(5):055006, Apr. 2019. doi:10.1088/1361-665X/ab0ea2.
- [3] M. M. J. Opgenoord and K. E. Willcox. Design for additive manufacturing: cellular structures in early-stage aerospace design. *Structural and Multidisciplinary Optimization*, 60(2):411–428, Aug. 2019. doi:10.1007/s00158-019-02305-8.
- [4] M. P. Bendsøe. Optimal shape design as a material distribution problem. *Structural optimization*, 1(4):193–202, Dec. 1989. doi:10.1007/BF01650949.

-
- [5] M. P. Bendsøe and O. Sigmund. *Topology Optimization*. Springer Berlin Heidelberg, Berlin, Heidelberg, 2004. doi:10.1007/978-3-662-05086-6.
- [6] W. S. Dorn, R. E. Gomory, and H. Greenberg. Automatic design of optimal structures. *J. Mécanique*, 1964.
- [7] M. Gilbert and A. Tyas. Layout optimization of large-scale pin-jointed frames. *Engineering Computations*, 20(8):1044–1064, Dec. 2003. doi:10.1108/02644400310503017.
- [8] J. Wu, O. Sigmund, and J. P. Groen. Topology optimization of multi-scale structures: a review. *Structural and Multidisciplinary Optimization*, Mar. 2021. doi:10.1007/s00158-021-02881-8.
- [9] K. Wu, O. Sigmund, and J. Du. Design of metamaterial mechanisms using robust topology optimization and variable linking scheme. *Structural and Multidisciplinary Optimization*, 63(4):1975–1988, Apr. 2021. doi:10.1007/s00158-020-02791-1.
- [10] A. Verbart, M. Langelaar, and F. v. Keulen. A unified aggregation and relaxation approach for stress-constrained topology optimization. *Structural and Multidisciplinary Optimization*, 55(2):663–679, Feb. 2017. doi:10.1007/s00158-016-1524-0.
- [11] W. Zhang and S. Sun. Scale-related topology optimization of cellular materials and structures. *International Journal for Numerical Methods in Engineering*, 68(9):993–1011, 2006. doi:10.1002/nme.1743.
- [12] W. Achtziger and C. Kanzow. Mathematical programs with vanishing constraints: optimality conditions and constraint qualifications. *Mathematical Programming*, 114(1):69–99, July 2008. doi:10.1007/s10107-006-0083-3.
- [13] G. Rozvany. On design-dependent constraints and singular topologies. *Structural and Multidisciplinary Optimization*, 21(2):164–172, Apr. 2001. doi:10.1007/s001580050181.
- [14] M. Stolpe. *On Models and Methods for Global Optimization of Structural Topology*. PhD thesis, KTH, 2003.
- [15] G. Sved and Z. Ginos. Structural optimization under multiple loading. *International Journal of Mechanical Sciences*, 10(10):803–805, Oct. 1968. doi:10.1016/0020-7403(68)90021-0.
- [16] G. Kreisselmeier and R. Steinhauser. Systematic Control Design by Optimizing a Vector Performance Index. *IFAC Proceedings Volumes*, 12(7):113–117, Sept. 1979. doi:10.1016/S1474-6670(17)65584-8.
- [17] P. Duysinx and M. P. Bendsøe. Topology optimization of continuum structures with local stress constraints. *International Journal for Numerical Methods in Engineering*, 43(8):1453–1478, 1998. doi:10.1002/(SICI)1097-0207(19981230)43:8<1453::AID-NME480>3.0.CO;2-2.

-
- [18] C. Le, J. Norato, T. Bruns, C. Ha, and D. Tortorelli. Stress-based topology optimization for continua. *Structural and Multidisciplinary Optimization*, 41(4):605–620, Apr. 2010. doi:10.1007/s00158-009-0440-y.
- [19] G. Cheng and Z. Jiang. Study on Topology Optimization with Stress Constraints. *Engineering Optimization*, 20(2):129–148, Nov. 1992. doi:10.1080/03052159208941276.
- [20] M. P. Bendsøe and O. Sigmund. Material interpolation schemes in topology optimization. *Archive of Applied Mechanics*, 69(9):635–654, Nov. 1999. doi:10.1007/s004190050248.
- [21] E. Andreassen, A. Clausen, M. Schevenels, B. S. Lazarov, and O. Sigmund. Efficient topology optimization in MATLAB using 88 lines of code. *Structural and Multidisciplinary Optimization*, 43(1):1–16, Jan. 2011. doi:10.1007/s00158-010-0594-7.
- [22] F. Wang, B. S. Lazarov, and O. Sigmund. On projection methods, convergence and robust formulations in topology optimization. *Structural and Multidisciplinary Optimization*, 43(6):767–784, June 2011. doi:10.1007/s00158-010-0602-y.
- [23] F. Ferrari and O. Sigmund. A new generation 99 line Matlab code for compliance Topology Optimization and its extension to 3D. *arXiv:2005.05436 [cs, math]*, July 2020.
- [24] K. Svanberg. The method of moving asymptotes—a new method for structural optimization. *International Journal for Numerical Methods in Engineering*, 24(2):359–373, 1987. doi:https://doi.org/10.1002/nme.1620240207.
- [25] O. Sigmund. Morphology-based black and white filters for topology optimization. *Structural and Multidisciplinary Optimization*, 33(4):401–424, Apr. 2007. doi:10.1007/s00158-006-0087-x.
- [26] K. Ejlebjerg Jensen. Anisotropic Mesh Adaptation and Topology Optimization in Three Dimensions. *Journal of Mechanical Design*, 138(6), June 2016. doi:10.1115/1.4032266.
- [27] O. Sigmund, N. Aage, and E. Andreassen. On the (non-)optimality of Michell structures. *Structural and Multidisciplinary Optimization*, 54(2):361–373, Aug. 2016. doi:10.1007/s00158-016-1420-7.
- [28] N. Aage, E. Andreassen, B. S. Lazarov, and O. Sigmund. Giga-voxel computational morphogenesis for structural design. *Nature*, 550(7674):84–86, Oct. 2017. doi:10.1038/nature23911. Number: 7674 Publisher: Nature Publishing Group.
- [29] A. G. M. Michell. The limits of economy of material in frame-structures. *The London, Edinburgh, and Dublin Philosophical Magazine and Journal of Science*, 8(47):589–597, Nov. 1904. doi:10.1080/14786440409463229.
- [30] E. Parkes. Joints in optimum frameworks. *International Journal of Solids and Structures*, 11(9):1017–1022, Sept. 1975. doi:10.1016/0020-7683(75)90044-X.

-
- [31] S. Diamond and S. Boyd. CVXPY: A Python-Embedded Modeling Language for Convex Optimization, 2016.
- [32] L. He, M. Gilbert, and X. Song. A Python script for adaptive layout optimization of trusses. *Structural and Multidisciplinary Optimization*, 60(2):835–847, Aug. 2019. doi:10.1007/s00158-019-02226-6.